EurJIC European Journal of Inorganic Chemistry

DOI: 10.1002/ejic.201200064

Simple Tuning of the Optoelectronic Properties of Ir^{III} and Pt^{II} Electrophosphors Based on Linkage Isomer Formation with a Naphthylthiazolyl Moiety

Xianbin Xu,[a] Yongbiao Zhao,[b] Jingshuang Dang,[c] Xiaolong Yang,[a] Guijiang Zhou,*[a] Dongge Ma,*[b] Lixiang Wang,[b] Wai-Yeung Wong,*[d] Zhaoxin Wu,*[e] and Xiang Zhao*[c]

Keywords: Iridium / Platinum / N,S ligands / Luminescence / Electrophosphors / Organic light-emitting diodes

By tuning the substitution position of a thiazolyl group on the naphthalene system (α or β site), the distinctive electronic structures associated with these functional ligands have a substantial influence on both the photophysical behavior and electroluminescent (EL) performance of the resulting linkage isomers for two series of Ir^{III} and Pt^{II} phosphorescent emitters. The photoluminescence wavelength can be redshifted by ca. 23 nm for the linkage isomers upon replacing the β-substituted thiazolyl-based ligand with its α-substituted counterpart in the homoleptic series of Ir^{III} phosphors. Furthermore, the bathochromic effect can be as much as ca. 42 nm for the heteroleptic Ir^{III} phosphors and ca. 59 nm for the Pt^{II} compounds. Similarly, metallophosphors that bear β-substituted ligands exhibit a different EL performance with respect to that of their linkage isomers with α-substituted ligands. The best EL results associated with the triplet emitters chelated with β-substituted ligands show a maximum brightness (L_{max}) of 22563 cd m^{-2}, an external quantum efficiency (η_{ext}) of 12.88 %, a luminance efficiency (η_L) of 30.84 cd A^{-1}, and a power efficiency (η_p) of 26.17 lm W^{-1}, whereas the EL performance of their α-counterparts was characterized by a peak L_{max} of 8653 cd m^{-2}, η_{ext} of 6.18 %, η_L of 8.55 cd A^{-1}, and η_p of 6.54 lm W^{-1}. Owing to its unique electronic structure, the thiazolyl group is a good alternative to the pyridyl moiety to improve the EL performance of the metallophosphor. We have also demonstrated a simple and useful route to tune the functional properties of cyclometalated triplet emitters for EL applications.

Introduction

With the unique attributes associated with organic light-emitting diodes (OLEDs), such as thin-film formation, high contrast, low weight, fast response, wide-view angle, and low power consumption, OLEDs are recognized as one of the best candidates for flat-panel display technologies, which are capable of meeting the most stringent demands of future display applications,[1] and energy-saving solid-state lighting sources.[2] Among the light-emitting materials available, phosphorescent (triplet) emitters are of prime importance because of their ability to harness both singlet and triplet excitons for light emission, which can ensure nearly 100% internal quantum efficiency.[3,4] Hence, the guest for phosphorescent emitters represents one of the milestones in the field of organic electroluminescence (EL), which holds great promise to bring organic EL devices into practical application. In this regard, tuning the photophysical and EL behavior of these phosphors are critical for the new generation of full-color displays or future solid-state light sources.[5] Unfortunately, this process is usually hindered by the tedious preparative synthetic work involved. Hence, the development of simple strategies to tune the photophysical and EL properties of triplet emitters is indispensable to the advancement of this field.

Recently, the functionalization of triplet emitters, especially for Ir^{III} and Pt^{II} ppy-type (Hppy = 2-phenylpyridine) complexes, has shown potential for the preparation of highly efficient triplet emitters.[6] Generally, functional moieties, such as triphenylamine,[6b–6d] carbazole,[6e,6h–6i] and

[a] MOE Key Laboratory for Nonequilibrium Synthesis and Modulation of Condensed Matter and Department of Chemistry, Faculty of Science, Xi'an Jiaotong University,
Xi'an 710049, P.R. China
Fax: +86-29-82663914
E-mail: zhougj@mail.xjtu.edu.cn
[b] State Key Laboratory of Polymer Physics and Chemistry Changchun Institute of Applied Chemistry, Chinese Academy of Sciences,
Changchun 130022, P.R. China
Fax: +86-431-5684-937
E-mail: mdg1014@ciac.jl.cn
[c] Institute for Chemical Physics and Department of Chemistry, Faculty of Science, Xi'an Jiaotong University,
Xi'an 710049, P.R. China
Fax: +86-29-82663914
E-mail: xzhao@mail.xjtu.edu.cn
[d] Institute of Molecular Functional Materials, Department of Chemistry and Institute of Advanced Materials, Hong Kong Baptist University,
Waterloo Road, Kowloon Tong, Hong Kong, P.R. China
Fax: +852-3411-7348
E-mail: rwywong@hkbu.edu.hk
[e] Key Laboratory for Physical Electronics and Devices of the Ministry of Education, Faculty of Electronic and Information Engineering, Xi'an Jiaotong University,
Xi'an 710049, P.R. China
Fax: +86-29-82664867
E-mail: zhaoxinwu@mail.xjtu.edu.cn

Supporting information for this article is available on the WWW under http://dx.doi.org/10.1002/ejic.201200064.

oxadiazole,[6f] can be introduced to the ppy ligand to give site-isolation and charge-carrier injection/transport features to the triplet emitters. From the outstanding EL performance of the as-prepared functionalized phosphorescent emitters, it is possible to bring about high-performance materials by using such a protocol. Based on the structural and electronic features of these functionalized Ir^{III} and Pt^{II} ppy-type triplet emitters, we can usually tailor the phenyl ring of ppy by chemical means to synthesize various functionalized organic ligands to prepare Ir^{III} and Pt^{II} phosphors.[6] As reported in the literature, the electronic structure of the pyridyl moiety can play a critical role to determine the overall photoelectronic behavior of the emitter.[7] This hints that changing the chemical structure of the phosphor represents another viable way to prepare a highly efficient triplet emitter. So, it would be attractive to develop some high-performance triplet emitters by modifying the pyridyl ring in ppy-type ligands. Here, we describe a series of Ir^{III} and Pt^{II} phosphors that bear functional ligands with the thiazolyl moiety substituted at different sites of the naphthalene, i.e. they exist as linkage isomers. Different to the commonly used electron-deficient pyridyl group, thiazole,[8] which can be regarded as a hybrid of pyridine and thiophene, is relatively underexplored in phosphorescent cyclometalate chemistry. The more electron-rich character of thiazole with respect to pyridine makes the thiazolyl system more reluctant to accept electrons from the chelated phenyl ring compared to its pyridyl counterpart. Accordingly, the unique electronic structure of thiazole would confer distinct properties to these new Ir^{III} and Pt^{II} phosphors. Furthermore, simply changing the substitution site of the thiazolyl group on naphthalene can markedly alter the photophysical and EL behavior of the resulting phosphors, which provides a very simple strategy to tune the optoelectronic properties of Ir^{III} and Pt^{II} phosphors whose decent EL performance indicates their potential in EL applications.

Results and Discussion

Synthetic Strategies and Structural Characterization

The chemical structures and detailed synthetic protocols of the Ir^{III} and Pt^{II} complexes are shown in Figure 1. The organic cyclometalating ligands **L1** and **L2** were prepared by the Suzuki coupling of 2-bromothiazole and the corresponding naphthylboronic acid in high yield. The homoleptic complexes **Ir-1** and **Ir-2** were prepared by the reaction of the ligand (**L1** and **L2**, respectively) with [$Ir(acac)_3$] at ca. 250 °C.[6b,7b] The heteroleptic congeners **Ir-3**, **Ir-4**, **Pt-1**, and **Pt-2** were obtained by a two-step procedure. The ligands reacted with the metal source ($IrCl_3 \cdot nH_2O$ or K_2PtCl_4) to afford chloride-bridged precursor complexes, which were then converted into the final heteroleptic complexes by reaction with acetylacetone in the presence of Na_2CO_3.[7a,9] These air-stable compounds were isolated in high purity as orange to red solids by column chromatography on silica gel with the appropriate eluent.

The stereochemical structure of **Ir-1** as a facial isomer with an inherent C_3 symmetry was confirmed by ^1H and ^{13}C NMR spectroscopy, which show that the three ligands

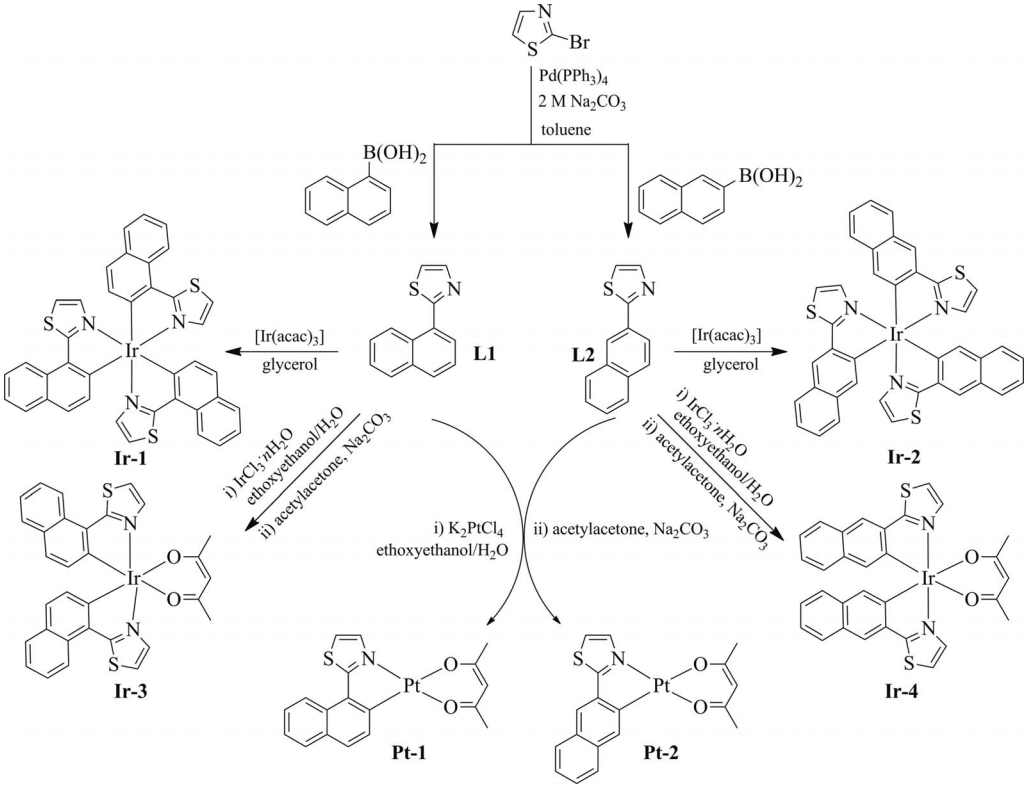

Figure 1. Synthesis of the new thiazole-based Ir^{III} and Pt^{II} complexes.

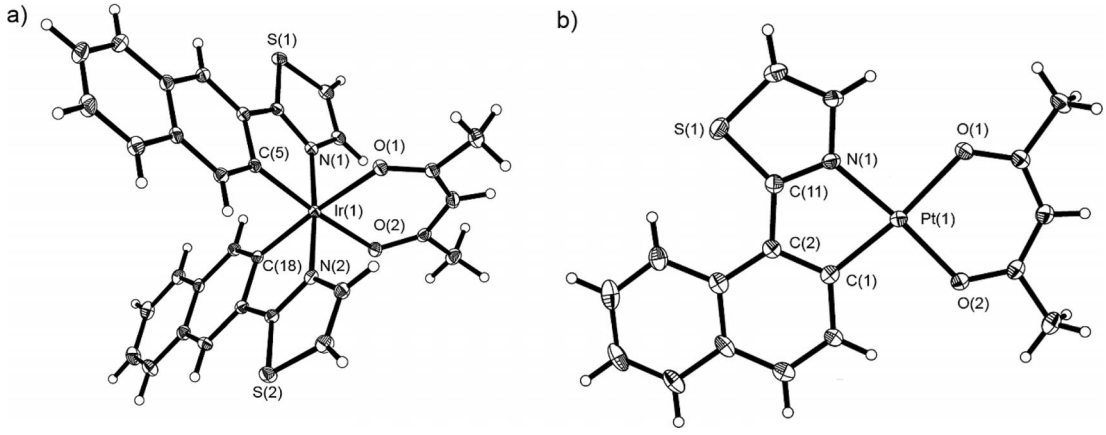

Figure 2. ORTEP drawings of a) **Ir-4** and b) **Pt-1** with thermal ellipsoids drawn at the 20% probability level. Labels on both the carbon atoms (except for those bonded to Ir and Pt) and the hydrogen atoms are omitted for clarity.

are magnetically equivalent. The poor solubility of **Ir-2** precluded its satisfactory NMR spectroscopic characterization. The structures of heteroleptic **Ir-3**, **Ir-4**, **Pt-1**, and **Pt-2** were also identified by the characteristic resonance peaks associated with the corresponding ligand and acetylacetone in their NMR spectra. In each case, the FAB-MS revealed the respective molecular ion peak. Presumably owing to the amorphous nature of these complexes, all attempts to obtain single crystals met with little success except for **Ir-4** and **Pt-1**. The X-ray crystal structures of **Ir-4** and **Pt-1** are depicted in Figure 2. For **Ir-4**, the metal center is coordinated by two anionic cyclometalated C^N ligands (**L2**) and one chelating acac$^-$ anion. The coordination pattern around the Ir center is distorted octahedral, with a *cis*-O,O, *cis*-C,C, and *trans*-N,N chelate arrangement (Tables S1 and S2 in the Supporting Information). The lengths of the bonds around the Ir center are typical compared with those in similar complexes.[6k] The X-ray crystal structure of **Pt-1** revealed that the Pt^{II} cation is coordinated by one anionic C^N ligand and an acetylacetone anion. The coordination arrangement around the Pt center consists of a distorted square-planar geometry with bond angles N(1)–Pt(1)–O(2) 175.2(2)°, C(1)–Pt(1)–O(1) 173.10(2)°, N(1)–Pt(1)–C(1) 80.90(2)°, and O(1)–Pt(1)–O(2) 92.6(2)°. Different from other structurally characterized Pt^{II}(C^N)(acac) complexes in which the molecules usually pack as dimers in a head-to-tail pattern in the asymmetric unit (Pt···Pt 3.15–3.76 Å), there is only one unique discrete molecule per asymmetric unit in the unit cell of **Pt-1**, which indicates a negligible Pt···Pt interaction between the individual molecules. **Pt-1** possesses a mean Pt–C bond length of 1.959(6) Å. The bond length of Pt–N [1.972(5) Å] is slightly longer than normal due to the weak *trans* influence exerted by the opposite acac O atom.[10] The Pt–O bond lengths are in the range of 1.998(4)–2.066(4) Å, which resemble those from other cyclometalated Pt(β-diketonato) complexes.[11]

Thermal and Photophysical Properties

The thermal properties of these thiazole-based complexes were characterized by thermogravimetric analysis (TGA) and differential scanning calorimetry (DSC) under a nitrogen flow. The TGA data reveal their good thermal stability with the 5% weight-reduction temperatures ($\Delta T_{5\%}$) ranging from 224–475 °C (Table 1). The thermal stability of **Pt-1** and **Pt-2** (227 and 224 °C, respectively) is inferior to that of **Ir-3** and **Ir-4** (356 and 310 °C, respectively). Without the ready-to-lose acetylacetonate auxiliary ligand, homoleptic **Ir-1** and **Ir-2** showed noticeably higher decomposition

Table 1. Photophysical, electrochemical, and thermal data for the new thiazole-based complexes.

	Absorption (293 K)[a] λ_{abs} /nm	Emission λ_{em} /nm 293 K	Φ_p[b]	τ_p[c] /μs	τ_r[d] /μs	$\Delta T_{5\%}/T_g$ /°C
Ir-1	242 (4.67), 264 (4.55), 303 (4.55), 327 (4.28), 342 (4.31), 408 (4.08), 450 (3.87), 488 (3.56)	593	0.08	0.69	8.63	475/152
Ir-2	225 (4.71), 277 (4.73), 292 (4.59), 321 (4.50), 344 (4.38), 419 (3.57) 483 (3.22)	570	0.06	0.45	7.50	460/145
Ir-3	229 (4.63), 272 (4.48), 303 (4.45), 337 (4.27), 366 (4.09), 408 (3.75), 458 (3.67), 496 (3.65)	608	0.07	0.68	9.71	356/160
Ir-4	227 (4.84), 256 (4.62), 285 (4.61), 299 (4.65), 316 (4.71), 356 (4.12), 409 (3.72), 485 (3.43)	566	0.12	0.57	4.75	310/153
Pt-1	232 (4.40), 259 (4.27), 270 (4.29), 303 (4.06), 329 (4.01), 347 (4.02), 384 (3.83), 426 (3.60), 450 (3.51)	609	0.02	0.81	40.50	227/130
Pt-2	226 (4.51), 260 (4.33), 276 (4.40), 292 (4.55), 323 (4.19), 340 (4.17), 376 (3.87), 433 (3.28)	550	0.04	1.08	27.00	224/135

[a] Measured in CH_2Cl_2 at a concentration of 10^{-5} M, and logε values are shown in parentheses. [b] In degassed CH_2Cl_2 relative to *fac*-[Ir(ppy)$_3$] (Φ_p = 0.40), λ_{ex} = 360 nm. [c] Measured in freeze–pump–thaw degassed CH_2Cl_2 solutions at a sample concentration of ca. 10^{-5} M, and the excitation wavelength was set at 355 nm for all the samples at 293 K. [d] The triplet radiative lifetimes (τ_r) were deduced from $\tau_r = \tau_p/\Phi_p$.

temperatures compared to those of heteroleptic **Ir-3**, **Ir-4**, **Pt-1**, and **Pt-2**. Analysis of the DSC traces for the complexes indicated their high glass-transition temperatures (T_g) in the range from 130 to 160 °C, which are desirable for high-performance OLEDs.

All of these phosphorescent complexes exhibit two noticeable absorption bands in their UV/Vis spectra (see part a of Figure 3 and Supporting Information, Figure S1). The strong UV absorption bands are assigned to the spin-allowed $S_1 \leftarrow S_0$ transitions of the organic ligands (i.e. $^1\pi$–π^* bands). The weaker, low-energy features are induced by both ^{1}MLCT$\leftarrow S_0$ and ^{3}MLCT$\leftarrow S_0$ (MLCT = metal-to-ligand charge transfer) excitations. The strong spin–orbit coupling effects induced by the heavy metal center are confirmed by the similar oscillator strengths (less than a factor of two in their extinction coefficients) for the two MLCT bands (Table 1).[7a] As indicated by the UV/Vis spectra (Figure 3, a), the complexes that bear a ligand with the thiazolyl group substituted at the α-position of naphthalene (i.e. **L1**) generally possess MLCT excited states of lower energy compared to those from their β-substituted congeners (i.e. **L2**) because **Ir-1**, **Ir-3**, and **Pt-1** exhibit bathochromically-shifted MLCT absorption bands with respect to those of **Ir-2**, **Ir-4**, and **Pt-2**, respectively (Table 1).

Under UV light irradiation at 360 nm, all of the complexes emit intense yellow–orange to red phosphorescence in CH_2Cl_2 (Table 1 and Figure 3, b). Their photoluminescence (PL) spectra have virtually identical line shapes, indicating that similar excited and/or ground states are involved in the phosphorescent transitions. The unstructured features associated with the PL spectra are suggestive of their predominantly MLCT character for the lowest triplet excited states (T_1) in all of these complexes at 293 K, which were confirmed by time-dependent (TD)-DFT calculations (Figure 4 and Table 2). Our TD-DFT calculations show that the lowest-energy transitions in these complexes correspond to HOMO→LUMO transitions with nonzero oscillator strengths and only the HOMO→LUMO transition is important for the first excited state (Table 2). From Table 2, the molecular orbital (MO) compositions represent the characters of both the S_1 and T_1 excited states in our systems. Therefore, the HOMO→LUMO transitions show the features of the lowest-energy excited state T_1, which is the origin of the emission in this series of complexes. As indicated by the contribution of metal d_π orbitals to the HOMO and LUMO (Table 2), the T_1 states involved in these complexes exhibit obvious MLCT characters, which

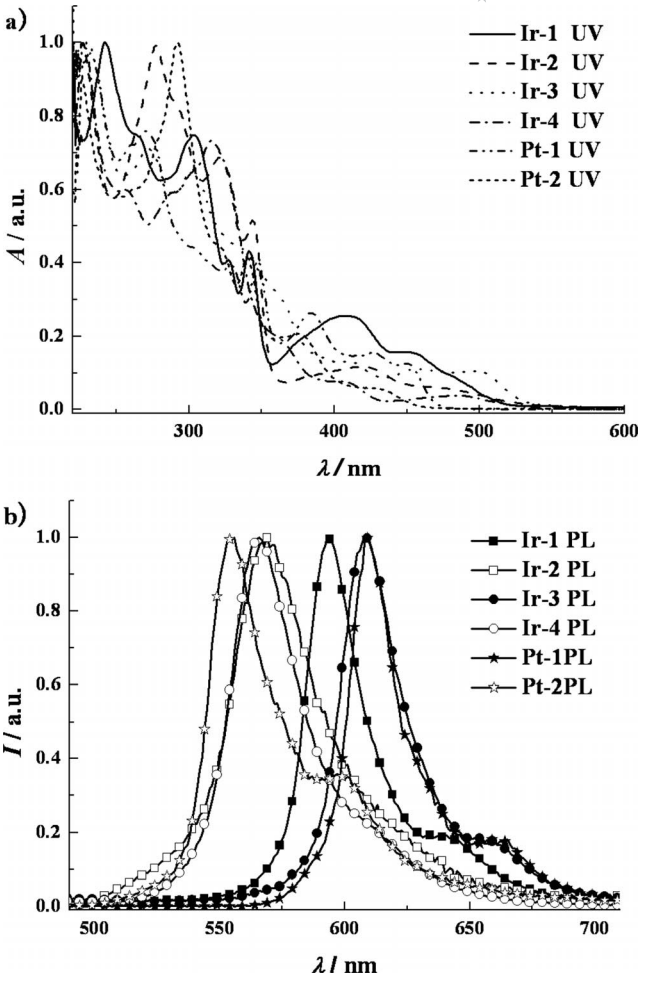

Figure 3. a) Absorption and b) PL spectra of the thiazole-based phosphors in CH_2Cl_2 at 293 K.

Table 2. Contribution of the metal d_π orbitals to the HOMO and LUMO together with the TD-DFT calculation results.

	Contribution of metal d_π orbitals to HOMO	Contribution of metal d_π orbitals to LUMO	The largest coefficient in the CI expansion of the T_1 state ($S_0 \rightarrow T_1$ exc. energy)[a]	The largest coefficient in the CI expansion of the S_1 state ($S_0 \rightarrow S_1$ exc. energy)[a]	The oscillator strength (*f*) of the $S_0 \rightarrow S_1$ transition
Ir-1	Ir 40.89%	Ir 0.17%	H→L: 0.57599 (602 nm)	H→L: 0.68337 (492 nm)	0.0223
Ir-2	Ir 48.22%	Ir 0.40%	H→L: 0.47280 (592 nm)	H→L: 0.65064 (543 nm)	0.0078
Ir-3	Ir 38.92%	Ir 3.49%	H→L: 0.57924 (607 nm)	H→L: 0.61910 (477 nm)	0.0404
Ir-4	Ir 47.61%	Ir 1.32%	H→L: 0.45001 (596 nm)	H→L: 0.61077 (519 nm)	0.0181
Pt-1	Pt 25.87%	Pt 4.82%	H→L: 0.74721 (619 nm)	H→L: 0.62862 (439 nm)	0.0706
Pt-2	Pt 34.16%	Pt 2.14%	H→L: 0.58644 (586 nm)	H→L: 0.65314 (468 nm)	0.0299

[a] H→L represents the HOMO to LUMO transition. CI = configuration interaction.

have been corroborated by the unstructured line shape of their PL spectra (Figure 3, b). In line with their UV behavior, the complexes of **L1** (**Ir-1**, **Ir-3**, and **Pt-1**) display longer emission wavelengths with respect to those of their counterparts with **L2** (**Ir-2**, **Ir-4** and **Pt-2**) due to the bathochromic effect observed for the MLCT absorption bands in **Ir-1**, **Ir-3**, and **Pt-1**. Although they share similar HOMO and LUMO characters (Figure 4), their MO patterns might not provide much useful information to explain this phenomenon. With reference to photophysical investigations in the literature,[6k,6l,7] the electronic structures of the organic ligands have a substantial influence on the photophysical behavior of their corresponding Ir^{III} and Pt^{II} ppy-type complexes. To find the origin of the PL behavior of our thiazole-based complexes, the MO patterns of the organic ligands were also obtained by theoretical computations (Figure 5). Despite the fact that **L1** and **L2** share similar MO patterns with the HOMO and LUMO located mainly on the π orbitals of the naphthyl and thiazolyl moieties, respectively, the electron density on the carbon atom chelated to the metal center is noticeably different. The chelated carbon atom in **L1** possesses a substantially higher electron density than that in **L2**, which indicates the electron-donating ability of the carbon atom in **L1**. Hence, it suggests that the metal center is chelated with electron-donating atoms in **Ir-1**, **Ir-3**, and **Pt-1**, which bear **L1**, whereas the situation is reversed in **Ir-2**, **Ir-4**, and **Pt-2** with **L2**. Accordingly, **L1**, which has an electron-donating chelating site, will facilitate the MLCT process that would stabilize the MLCT states in **Ir-1**, **Ir-3**, and **Pt-1**. As a result, a redshift was detected in the MLCT emission bands as well as in the corresponding absorption bands (Figure 3, b). By comparison of the analogous heteroleptic Ir^{III} complex with the naphthylpyridyl-derived cyclometalated ligand (which absorbs at 486 nm and emits at 590 nm),[3i,3j] **Ir-3** shows a notable bathochromic effect in both the absorption and emission features due to the presence of the thiazolyl ring.

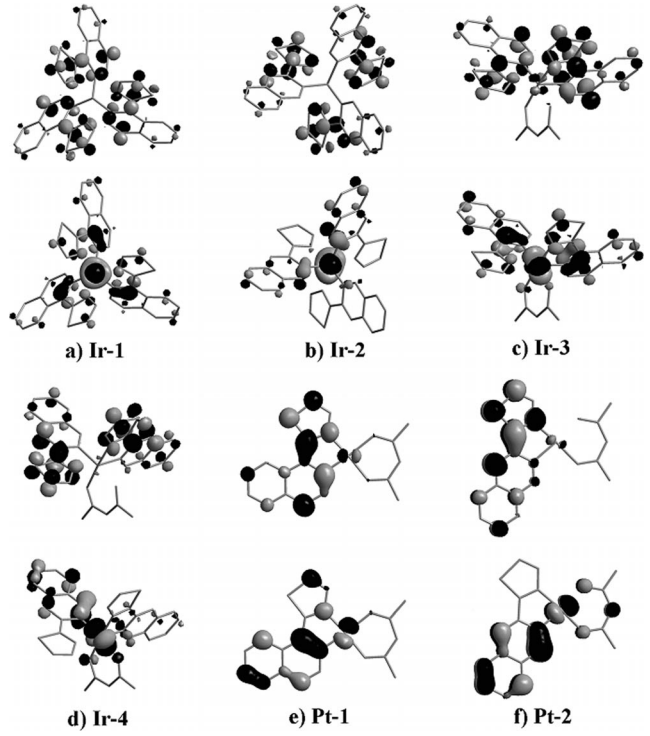

Figure 4. Plots of the LUMO (top) and HOMO (bottom) levels for each of the thiazole-based Ir^{III} and Pt^{II} complexes.

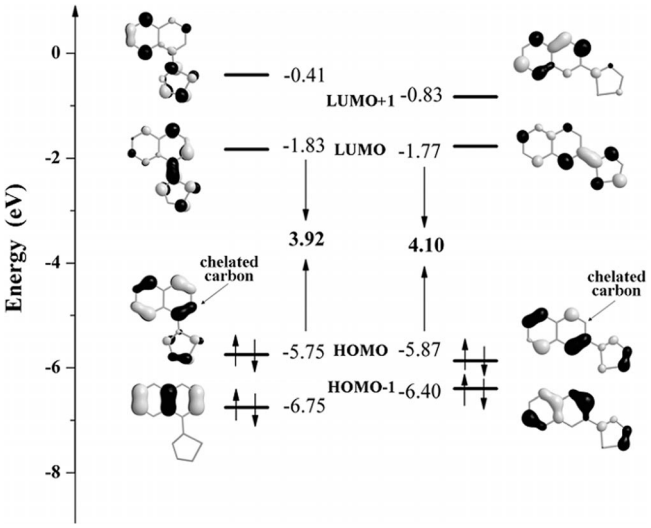

Figure 5. MO patterns and energy diagram for **L1** and **L2**.

Redox Properties

The redox properties of these thiazole-based complexes were investigated by cyclic voltammetry (CV) calibrated using ferrocene as the internal standard under a nitrogen atmosphere. The results are presented in Table 3. All of the iridium complexes gave reversible $E_{1/2}^{ox}$ values at around 0.4 V, which are akin to those of their analogs in the literature.[6b,6k] **Pt-1** and **Pt-2** exhibit two oxidation waves. The first reversible anodic wave can be assigned to the oxidation of electron-rich organic ligands, and the second irreversible wave is ascribed to the oxidation of the metal center as the square-planar Pt^{I} and Pt^{III} metal centers are susceptible to nucleophilic attack by solvents, which usually makes Pt^{II} redox processes irreversible.[11c] Furthermore, $[Pt(ppy)(en)]^{+}$ was also reported to have an irreversible oxidation wave at ca. 0.51 V,[12] close to 0.46 V for the second oxidation potential of **Pt-1** and **Pt-2**.

Table 3. Redox properties of the thiazole-based complexes.

	$E_{1/2}^{ox}$ /V	$E_{1/2}^{red}$ /V	HOMO /eV	LUMO /eV
Ir-1	0.40	–2.51, –2.71	–5.20	–2.29
Ir-2	0.30	–2.46	–5.10	–2.34
Ir-3	0.46	–2.42, –2.60, –2.74	–5.26	–2.38
Ir-4	0.38	–2.40, –2.52	–5.18	–2.40
Pt-1	0.22, 0.46[a]	–2.27	–5.02	–2.53
Pt-2	0.21, 0.46[a]	–2.26, –2.73	–5.01	–2.54

[a] Irreversible wave.

The first quasireversible reduction couple for all the complexes is located between –2.51 and –2.26 V, which indicates their noticeably lower LUMO levels compared with their

counterparts reported in the literature.[6b,6k] Generally, the LUMOs of complexes of this type mainly consist of the π orbitals of the nitrogen heterocycle in the ppy-type ligand. Different from other nitrogen heterocycles in typical ppy-type ligands, the thiazolyl moiety shows an electron-rich character, which makes it reluctant to accept electrons. Consequently, the LUMOs of these thiazole-based complexes are delocalized over a larger area with respect to those of the reported congeners, as confirmed by the MO patterns shown in Figure 4. The more delocalized pattern will stabilize the LUMOs of the complexes, thereby lowering the LUMO levels.[13] The low LUMO levels would facilitate the electron injection/transport (EI/ET) process of these complexes, which should benefit their EL performance. Therefore, we can see the impact of the thiazole moiety in tailoring the electronic properties of the metallophosphors.

Electrophosphorescence Characterization

Generally, a long-wavelength phosphorescent emitter shows good hole injection/transport (HI/HT) behavior. On the contrary, our new metallophosphors show EI/ET properties as indicated by their low LUMO levels, which are induced by the unique electronic traits of the thiazolyl-anchored system. Inspired by these special features of the thiazole-based phosphors, we have characterized their electrophosphorescent potential by fabricating doped phosphorescent OLEDs (PHOLEDs) with the configuration shown in Figure 6. 4,4′-*N*,*N*′-dicarbazolebiphenyl (CBP) was employed as the host material because of its ambipolar charge-carrier-transport properties. 4,4′-Bis[*N*-(1-naphthyl)-*N*-phenylamino]biphenyl (NPB) acts as a hole-transport layer together with the thin MoO_3 layer for hole-injection. 2,9-Dimethyl-4,7-diphenyl-1,10-phenanthroline (BCP) serves as a hole blocker. Tris(8-hydroxyquinolinato)aluminum (Alq_3) and LiF were employed to prepare the electron-transport and electron-injection layers, respectively. All of these functional materials were deposited onto the multilayer PHOLEDs with the structure of indium tin oxide (ITO)/MoO_3 (10 nm)/NPB (80 nm)/dopant:CBP (20 nm)/BCP (10 nm)/Alq_3 (30 nm)/LiF:Al (1:100 nm). In order to optimize the EL performance, doping-concentration-dependent experiments were also carried out.

When the appropriate voltage was applied, an intense yellow–orange to red light was emitted from each of the devices. From the EL spectra recorded at ca. 5 V, we can see clearly the resemblance of their line shape with that of the corresponding PL spectra (Figure 7 and Figure S2), which indicates that the EL arises from the triplet excited states of the phosphors. The performance data of these optimized EL devices are summarized in Table 4. For the devices with homoleptic iridium phosphors, even though the PL quantum yield of **Ir-2** is lower than that of **Ir-1**, device **B2** can show the maximum EL abilities with peak luminance (L_{max}) of 22563 cd m^{-2} at 15.9 V, current efficiency (η_L) of 30.84 cd A^{-1}, external quantum efficiency (η_{ext}) of

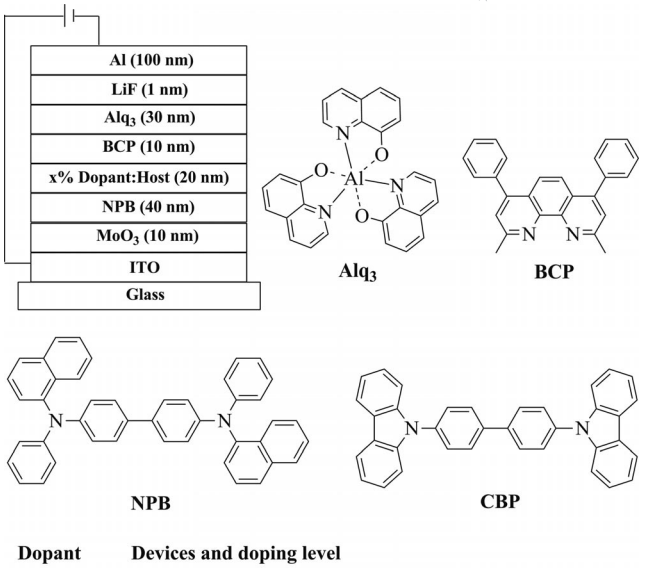

Dopant	Devices and doping level
Ir-1	**A1** (2 wt.-%), **A2** (5 wt.-%), **A3** (8 wt.-%), **A4** (13 wt.-%)
Ir-2	**B1** (2 wt.-%), **B2** (5 wt.-%), **B3** (8 wt.-%), **B4** (11 wt.-%)
Ir-3	**C1** (2 wt.-%), **C2** (5 wt.-%), **C3** (8 wt.-%), **C4** (11 wt.-%)
Ir-4	**D1** (1 wt.-%), **D2** (4 wt.-%), **D3** (7 wt.-%), **D4** (10 wt.-%)
Pt-1	**E1** (2 wt.-%), **E2** (5 wt.-%), **E3** (8 wt.-%), **E4** (11 wt.-%)
Pt-2	**F1** (2 wt.-%), **F2** (5 wt.-%), **F3** (9 wt.-%), **F4** (13 wt.-%)

Figure 6. General configuration of the electrophosphorescent OLEDs and the molecular structures of the compounds used in these devices.

12.88%, and power efficiency (η_P) of 26.17 lm W^{-1}, whereas the corresponding values of 8635 cd m^{-2} at 14.3 V, 8.55 cd A^{-1}, 6.18%, and 6.54 lm W^{-1} are associated with device **A3**. Employing the heteroleptic iridium emitters, device **D4** exhibits a better peak EL performance with L_{max} of 16849 cd m^{-2} at 17.9 V, η_L of 12.55 cd A^{-1}, η_{ext} of 5.26%, and η_P of 8.31 lm W^{-1} than device **C3** (6037 cd m^{-2} at 13.9 V, 3.55 cd A^{-1}, 3.98%, and 2.86 lm W^{-1}). However, device **C3** shows better EL characteristics than the device made with the naphthylpyridyl-based iridium congener as the dopant (peak efficiencies of 0.47 cd A^{-1} and 1.3% at

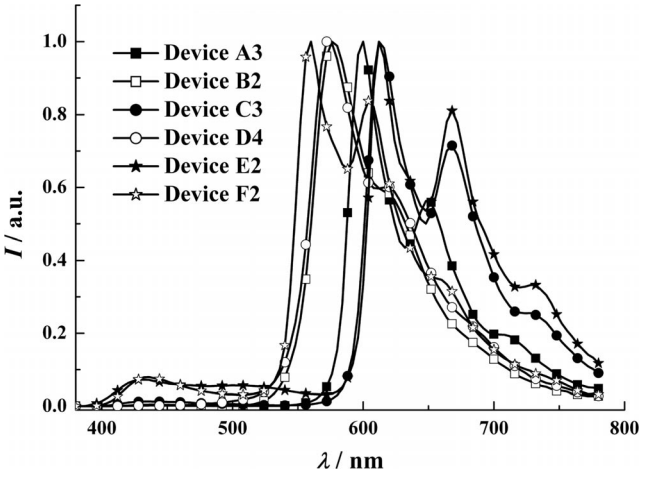

Figure 7. EL spectra for the optimized electrophosphorescent OLEDs at ca. 5 V.

Table 4. The EL performance of the optimized electrophosphorescent OLEDs.

Device	Phosphor dopant	$V_{turn\text{-}on}$ /V	L_{max} /cd m^{-2} [a]	η_{ext} /%	η_L /cd A^{-1}	η_P /lm W^{-1}	λ_{max} /nm [d]
A3	**Ir-1** (8.0 wt.-%)	3.9	8635 (14.3)	6.18 (4.3) [a]	8.55 (4.3)	6.54 (4.1)	600 (0.64, 0.36)
				5.89 [b]	8.13	4.11	
				5.00 [c]	6.89	2.21	
B2	**Ir-2** (5.0 wt.-%)	3.5	22563 (15.9)	12.88 (3.7)	30.84 (3.7)	26.17 (3.7)	576 (0.55, 0.45)
				9.67	23.17	13.27	
				8.06	19.28	7.09	
C3	**Ir-3** (8.0 wt.-%)	3.9	6037 (13.9)	3.98 (3.9)	3.55 (3.9)	2.86 (3.9)	612 (0.66, 0.32)
				3.33	2.94	1.28	
				2.67	2.36	0.69	
D4	**Ir-4** (10.0 wt.-%)	3.5	16849 (17.9)	5.26 (5.3)	12.55 (5.3)	8.31 (4.5)	572 (0.54, 0.46)
				5.08	12.13	6.16	
				3.97	9.49	2.82	
E2	**Pt-1** (5.0 wt.-%)	5.3	1165 (14.5)	0.95 (6.5)	0.77 (6.5)	0.38 (0.63)	612 (0.58, 0.31)
				0.82	0.68	0.21	
				0.57	0.52	0.11	
F2	**Pt-2** (5.0 wt.-%)	3.5	3979 (14.3)	3.18 (3.9)	6.67 (5.3)	5.24 (3.7)	560 (0.50, 0.45)
				2.44	5.86	2.97	
				1.20	2.85	0.86	

[a] Maximum values of the devices. Values in parentheses are the voltages at which they were obtained. [b] Values were collected at 100 cd m^{-2}. [c] Values collected at 1000 cd m^{-2}. [d] Values were collected at 5 V and CIE coordinates (x, y) are shown in parentheses.

40 cd m^{-2}).[3i] Therefore, it is apparent that the thiazolyl moiety improved the EL performance of the electrophosphors. For the devices with platinum-based triplet emitters, device **F2** with L_{max} of 3979 cd m^{-2} at 14.3 V, η_L of 6.67 cd A^{-1}, η_{ext} of 3.18%, and η_P of 5.24 lm W^{-1} outperformed device **E2** (L_{max} of 1165 cd m^{-2} at 14.5 V, η_L of 0.77 cd A^{-1}, η_{ext} of 0.95%, and η_P of 0.38 lm W^{-1}). Furthermore, devices **B2**, **D4**, and **F2** generally give higher luminance compared with devices **A3**, **C3**, and **E2** in their current-density–voltage–luminance (J–V–L) curves (Figure 8). Hence, devices **B2**, **D4**, and **F2**, with emitters that bear **L2**, exhibit noticeably better EL potential over devices **A3**, **C3**, and **E2**, with emitters that possess **L1** (Table 4). Given the same device configuration to that of devices **A3**, **C3**, and **E2**, the better EL performance associated with devices **B2**, **D4**, and **F2** is attributed to the unique electronic features of their emitters (**Ir-2**, **Ir-4**, and **Pt-2**), which show higher HOMO and lower LUMO levels (Table 3) with respect to **Ir-1**, **Ir-3**, and **Pt-1**, respectively. This indicates that **Ir-2**, **Ir-4**, and **Pt-2** possess more balanced charge-carrier injection/transport features than **Ir-1**, **Ir-3**, and **Pt-1**, respectively, resulting in the improved EL performance for devices **B2**, **D4**, and **F2**. Remarkably, by changing the substitution position of the thiazolyl group on naphthalene, we were able to tune the EL properties of the triplet emitters. The dependence of the EL efficiency on luminance for all the devices is given in Figure S4. The adverse efficiency roll-off effect due to either triplet–triplet annihilation or excited-state saturation only becomes important at a luminance level beyond 1000 cd m^{-2}, which is likely attributed to the favorably short phosphorescent lifetime ($\leq$ 1 μs) of the phosphors concerned (Table 1).

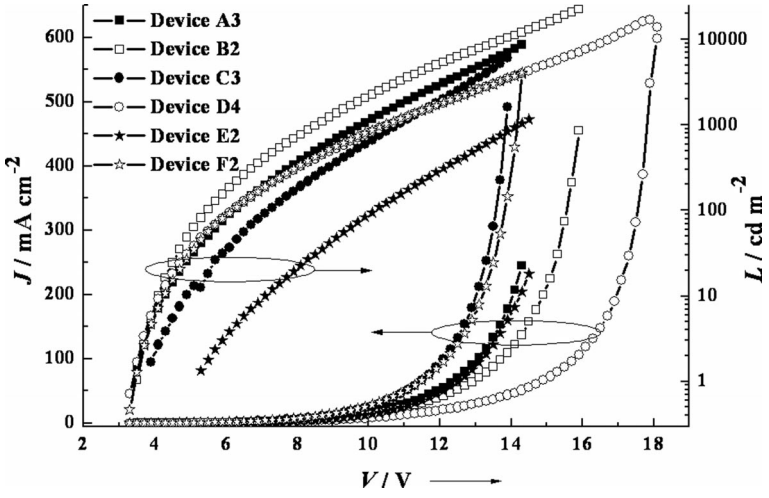

Figure 8. J–V–L curves for the optimized electrophosphorescent OLEDs.

Conclusions

A series of robust thiazole-based cyclometalated Ir^{III} and Pt^{II} long-wavelength-emitting phosphors have been synthesized and fully characterized. By both the introduction of a thiazole moiety to the ppy-type ligands and changing its substitution position on naphthalene, the corresponding phosphorescent complexes exhibit not only color-tuning capability but also unique charge-carrier injection/transport behavior, which favors their EL properties. Significant distinctions were found for the photophysical and electrophosphorescent properties of these linkage isomers, even though they have similar cyclometalated frameworks. Triplet emitters chelated with β-substituted naphthylthiazolyl ligands give impressive peak efficiencies at η_{ext} of 12.88%, η_L of 30.84 cd A^{-1}, and η_p of 26.17 lm W^{-1}, which are superior to those of the α-substituted counterparts. Furthermore, the replacement of the pyridyl group with a thiazolyl moiety in the cyclometalated ligand generally led to an improvement in the EL performance of the metallophosphor. Based on these results, we think that the introduction of a thiazole group to functionalized organic ligands for the preparation of cyclometalated Ir^{III} and Pt^{II} phosphors has great potential to meet the requirements for EL applications.

Experimental Section

General Information: All reactions were conducted under a nitrogen atmosphere and no special precautions were required during workup. Solvents were carefully dried and distilled from appropriate drying agents prior to use. Commercially available reagents were used without further purification unless otherwise stated. All reactions were monitored by TLC with Merck precoated aluminum plates. Flash column chromatography was carried out using silica gel (200–300 mesh). FAB mass spectra were recorded with a Finnigan MAT SSQ710 system. NMR spectra were measured in $CDCl_3$ with a Bruker AXS 400 MHz spectrometer with the chemical shifts quoted relative to tetramethylsilane.

Physical Measurements: UV/Vis spectra were recorded with a Shimadzu UV-2250 spectrophotometer. The photoluminescent properties of the complexes were measured with a Hitachi F-4500 fluorescence spectrophotometer. The phosphorescence quantum yields were determined in degassed CH_2Cl_2 solution at 293 K against the *fac*-[Ir(ppy)$_3$] standard (Φ_P = 0.40).[14] The lifetimes were measured with a single photon counting spectrometer from Edinburgh Instruments (FLS920) with a hydrogen-filled pulse lamp as the excitation source. The data analysis was conducted by iterative convolution of the luminescence decay profile with the instrument response function using the software package provided by Edinburgh Instruments. DSC was performed with a NETZSCH DSC 200 PC unit under a nitrogen flow at a heating rate of 10 °C min^{-1}. TGA was conducted with a NETZSCH STA 409C instrument under nitrogen with a heating rate of 20 °C min^{-1}. Electrochemical measurements were performed using a Princeton Applied Research model 273A potentiostat. Cyclic voltammetry of the sample solutions was performed at a scan rate of 100 mV s^{-1} using a glassy carbon working electrode, a platinum counter electrode, and a platinum-wire reference electrode. The solvent was deoxygenated tetrahydrofuran, and the supporting electrolyte was 0.1 M [nBu$_4$N][PF_6]. Ferrocene was added as a calibrant after each set of measurements, and all potentials reported were quoted with reference to the ferrocene–ferrocenium couple ($E_{1/2}$ = +0.27 V relative to the reference electrode). The oxidation (E_{ox}) and reduction (E_{red}) potentials were used to determine the HOMO and LUMO energy levels using the equations E_{HOMO} = –(E_{ox} + 4.8) eV and E_{LUMO} = –(E_{red} + 4.8) eV which were calculated using the internal standard ferrocene value of –4.8 eV with respect to the vacuum level.[15]

General Procedure for the Synthesis of L1 and L2: Under an inert atmosphere, 2-bromothiazole and the corresponding naphthylboronic acid (1.2 equiv.) were added to toluene and 2 M Na_2CO_3 (1:1 v/v) with $Pd(PPh_3)_4$ (5 mol-%). The reaction mixture was heated to ca. 110 °C and stirred for 24 h. The reaction mixture was cooled to room temperature and extracted with CH_2Cl_2. The combined organic phase was dried with anhydrous $MgSO_4$. The volatile components were removed under reduced pressure to give a crude product, which was purified by column chromatography on silica gel eluting with CH_2Cl_2 and hexane (2:1, v/v). **L1** and **L2** were obtained in high yields of about 90%.

L1: Yield: 88%. ^{1}H NMR (400 MHz, $CDCl_3$): δ = 8.78–8.76 (m, 1 H, Ar), 8.02 (d, J = 3.6 Hz, 1 H, Ar), 7.94–7.88 (m, 2 H, Ar), 7.81 (dd, J = 7.2, 1.2 Hz, 1 H, Ar), 7.59–7.49 (m, 3 H, Ar), 7.43 (d, J = 3.2 Hz, 1 H, Ar) ppm. ^{13}C NMR (100 MHz, $CDCl_3$): δ = 133.97, 130.77, 130.58, 130.33, 128.58, 128.29, 127.27, 126.32, 125.77, 124.98, 119.64 ppm. FAB-MS: m/z = 211 $[M]^+$. $C_{13}H_9NS$ (211.28): calcd. C 73.90, H 4.29, N 6.63; found C 73.56, H 4.02, N 6.33.

L2: Yield: 90%. ^{1}H NMR (400 MHz, $CDCl_3$): δ = 8.44 (d, J = 1.2 Hz, 1 H, Ar), 8.07 (dd, J = 8.4, 1.6 Hz, 1 H, Ar), 7.93–7.89 (m, 3 H, Ar), 7.86–7.83 (m, 1 H, Ar), 7.53–7.49 (m, 2 H, Ar), 7.35 (d, J = 3.2 Hz, 1 H, Ar) ppm. ^{13}C NMR (100 MHz, $CDCl_3$): δ = 134.06, 133.25, 130.93, 128.74, 128.59, 127.79, 126.96, 126.74, 125.97, 124.03, 119.92 ppm. FAB-MS: m/z = 211 $[M]^+$. $C_{13}H_9NS$ (211.28): calcd. C 73.90, H 4.29, N 6.63; found C 73.68, H 4.22, N 6.23.

General Procedure for the Synthesis of Homoleptic Iridium(III) Complexes: Under an N_2 atmosphere, the cyclometalating ligand and [Ir(acac)$_3$] (approximately 0.25 equiv.) were heated to 230 °C in glycerol for 18 h. The reaction mixture was cooled to room temperature. To prepare **Ir-1**, water was added to the reaction mixture, which was then extracted with CH_2Cl_2. The organic phase was dried with anhydrous $MgSO_4$, and the solvent was removed under reduced pressure. The residue was chromatographed on a silica column by using CH_2Cl_2 and hexane (3:1 v/v) as eluent to afford a pure sample. To synthesize **Ir-2**, the dark red precipitate formed was collected by filtration, washed with ethanol and dried in vacuo. Each of the iridium(III) complexes was obtained in approximately 20% overall yield.

Ir-1: Yield: 20%. ^{1}H NMR (400 MHz, $CDCl_3$): δ = 8.40 (dd, J = 8.5, 0.6 Hz, 3 H, Ar), 7.75 (dd, J = 8.3, 0.9 Hz, 3 H, Ar), 7.57–7.53 (m, 3 H, Ar), 7.37–7.33 (m, 3 H, Ar), 7.27–7.20 (m, 9 H, Ar), 6.97 (d, J = 3.6 Hz, 3 H, Ar) ppm. ^{13}C NMR (100 MHz, $CDCl_3$): δ = 175.41, 167.92, 138.69, 137.21, 133.80, 130.39, 130.24, 130.00, 129.86, 126.83, 122.38, 121.27, 116.66 (Ar) ppm. FAB-MS: m/z = 823 $[M]^+$. $C_{39}H_{24}IrN_3S_3$ (823.04): calcd. C 56.91, H 2.94, N 5.11; found C 56.45, H 2.72, N 4.93.

Ir-2: Yield: 18%. FAB-MS: m/z = 823 $[M]^+$. $C_{39}H_{24}IrN_3S_3$ (823.04): calcd. C 56.91, H 2.94, N 5.11; found C 56.56, H 2.70, N 4.82.

General Procedure for the Synthesis of Heteroleptic Iridium(III) and Platinum(II) Complexes: Under an N_2 atmosphere, the cyclometalating ligand and $IrCl_3 \cdot nH_2O$ (0.5 equiv.) or K_2PtCl_4 (0.9 equiv.) were heated to 100 °C in a mixture of ethoxyethanol and water (3:1

v/v) for 18 h. The reaction mixture was cooled to room temperature, and water was added. The chloride-bridged precursor complexes were formed as colored precipitates, which were collected by filtration and dried in vacuo. The precursor complex, acetylacetone (5 equiv.), and Na_2CO_3 (10 equiv.) were added to ethoxyethanol under an inert atmosphere. The reaction mixture was heated to 100 °C for 16 h before it was cooled to room temperature. Water was added, and the crude product was collected. After chromatography on a silica column with the appropriate eluent, the complexes were obtained in approximately 30% overall yield.

Ir-3: Yield: 32%. ^{1}H NMR (400 MHz, $CDCl_3$): δ = 8.32 (dd, J = 8.4, 0.6 Hz, 2 H, Ar), 7.82 (d, J = 3.6 Hz, 2 H, Ar), 7.62 (d, J = 8.0 Hz, 1 H, Ar), 7.55 (d, J = 3.6 Hz, 2 H, Ar), 7.53–7.49 (m, 2 H, Ar), 7.28–7.24 (m, 2 H, Ar), 6.48 (d, J = 8.4 Hz, 2 H, Ar), 5.26 (s, 1 H, acac), 1.82 (s, 6 H, acac) ppm. ^{13}C NMR (100 MHz, $CDCl_3$): δ = 185.00 (acac), 176.12, 154.69, 138.57, 134.81, 132.88, 130.17, 129.99, 129.77, 129.48, 127.07, 122.50, 121.56, 115.84 (Ar), 100.46, 28.37 (acac) ppm. FAB-MS: m/z = 712 $[M]^+$. $C_{31}H_{23}IrN_2O_2S_2$ (711.87): calcd. C 52.30, H 3.26, N 3.94; found C 52.01, H 3.37, N 3.73.

Ir-4: Yield: 30%. ^{1}H NMR (400 MHz, $CDCl_3$): δ = 8.00 (s, 2 H, Ar), 7.80 (d, J = 3.5 Hz, 2 H, Ar), 7.58 (dd, J = 8.0, 0.6 Hz, 2 H, Ar), 7.50 (d, J = 3.5 Hz, 2 H, Ar), 7.29 (d, J = 8.2 Hz, 2 H, Ar), 7.18–7.14 (m, 2 H, Ar), 7.12–7.08 (m, 2 H, Ar), 6.61 (s, 2 H, Ar), 5.26 (s, 1 H, acac), 1.83 (s, 6 H, acac) ppm. ^{13}C NMR (100 MHz, $CDCl_3$): δ = 185.12 (acac), 177.60, 141.51, 140.05, 137.33, 134.99, 130.71, 129.65, 128.42, 126.53, 125.82, 123.37, 122.90, 117.14 (Ar), 100.47, 28.51 (acac) ppm. FAB-MS: m/z = 712 $[M]^+$. $C_{31}H_{23}IrN_2O_2S_2$ (711.87): calcd. C 52.30, H 3.26, N 3.94; found C 52.51, H 3.45, N 3.83.

Pt-1: Yield: 28%. ^{1}H NMR (400 MHz, $CDCl_3$): δ = 8.14 (dd, J = 8.4, 0.6 Hz, 1 H, Ar), 8.07 (d, J = 3.6 Hz, 1 H, Ar), 7.91 (d, J = 8.4 Hz, 1 H, Ar), 7.84 (d, J = 8.0 Hz, 1 H, Ar), 7.67 (d, J = 8.0 Hz, 1 H, Ar), 7.57–7.53 (m, 1 H, Ar), 7.43–7.39 (m, 2 H, Ar), 5.52 (s, 1 H, acac), 2.05 (s, 3 H, acac), 2.01 (s, 3 H, acac) ppm. ^{13}C NMR (100 MHz, $CDCl_3$): δ = 185.71, 183.81 (acac), 177.25, 144.00, 142.75, 137.48, 134.39, 131.56, 129.94, 129.07, 128.88, 127.54, 123.55, 121.68, 115.00 (Ar), 102.64, 28.01, 27.23 (acac) ppm. FAB-MS: m/z = 504 $[M]^+$. $C_{18}H_{15}NO_2PtS$ (504.47): calcd. C 42.86, H 3.00, N 2.78; found C 42.69, H 3.15, N 2.53.

Pt-2: Yield: 31%. ^{1}H NMR (400 MHz, $CDCl_3$): δ = 8.32 (d, J = 3.6 Hz, 1 H, Ar), 7.94 (s, 1 H, Ar), 7.90 (s, 1 H, Ar), 7.79 (d, J = 8.1 Hz, 1 H, Ar), 7.73 (d, J = 8.1 Hz, 1 H, Ar), 7.43–7.40 (m, 1 H, Ar), 7.35–7.32 (m, 2 H, Ar), 5.51 (s, 1 H, acac), 2.07 (s, 3 H, acac), 1.99 (s, 3 H, acac) ppm. ^{13}C NMR (100 MHz, $CDCl_3$): δ = 185.55, 183.84 (acac), 178.62, 140.21, 138.47, 134.38, 130.93, 129.37, 128.62, 128.24, 127.26, 127.23, 124.34, 122.88, 116.31 (Ar), 102.46, 28.02, 27.17 (acac) ppm. FAB-MS: m/z = 504 $[M]^+$. $C_{18}H_{15}NO_2PtS$ (504.47): calcd. C 42.86, H 3.00, N 2.78; found C 42.70, H 3.12, N 2.69.

X-ray Crystallography: X-ray diffraction data were collected at 293 K using graphite-monochromated Mo-K_α radiation (λ = 0.71073 Å) with a Bruker Axs SMART 1000 CCD diffractometer. The collected frames were processed with the software SAINT+[16] and an absorption correction (SADABS)[17] was applied to the collected reflections. The structure was solved by direct methods (SHELXTL)[18] in conjunction with standard difference Fourier techniques and subsequently refined by full-matrix least-squares analyses on F^2. Hydrogen atoms were generated in their idealized positions and all non-hydrogen atoms were refined anisotropically. CCDC-858592 (for **Ir-4**) and -858593 (for **Pt-1**) contain the supplementary crystallographic data for this paper. These data can be obtained free of charge from The Cambridge Crystallographic Data Centre via www.ccdc.cam.ac.uk/data_request/cif.

OLED Fabrication and Measurements: The precleaned ITO glass substrates were treated with ozone for 20 min. Poly(3,4-ethylenedioxythiophene) poly(styrenesulfonate)was deposited on the ITO surface by the spin-coating method to form a 40 nm-thick hole-injection layer after being cured at 120 °C for 30 min in air. The emitting layer (50 nm) was obtained by spin-coating a chloroform solution of each phosphorescent polymer dopant (x wt.-%) in CBP at various concentrations. The sample was dried in a vacuum oven at 50 °C for 15 min and transferred to the deposition system for organic and metal deposition. BCP (15 nm), Alq_3 (40 nm), LiF (1 nm), and Al cathode (100 nm) were successively evaporated at a base pressure less than 10^{-6} Torr. The EL spectra and CIE coordinates were measured with a PR650 spectra colorimeter. The J–V–L curves of the devices were recorded with a Keithley 2400/2000 source meter, and the luminance was measured using a PR650 SpectraScan spectrometer. All the experiments and measurements were carried out under ambient conditions.

Computational Details: DFT calculations were performed using the B3LYP functional. The basis set used for the C, H, N, and O atoms was 6-31G, whereas effective core potentials with a LanL2DZ basis set were employed for the P, Pt, and Ir atoms.[19] Polarization functions were added for P [ζ_d(P) = 0.340]. All calculations were carried out using the Gaussian 03 program.[20] Mulliken population analyses were performed using MullPop.[21] Frontier molecular orbitals obtained from the DFT calculations were plotted using the Molden 3.7 program.[22]

Supporting Information (see footnote on the first page of this article): Crystal data, bond lengths, and bond angles of **Ir-4** and **Pt-1**; UV/Vis spectra, EL spectra, *J-V-L* curves, and EL efficiency versus luminance curves for all phosphorescent OLEDs.

Acknowledgments

This work was supported by the Xi'an Jiaotong University (Tengfei Project), the Fundamental Research Funds for the Central Universities, a Research Grant from Shaanxi Province (research grant number 2009JQ2008), the National Natural Science Foundation of China (NSFC) (grant number 20902072), the Program for New Century Excellent Talents in University, and the Ministry of Education of China (NECT-09-0651). W.-Y. Wong acknowledges financial support from the Hong Kong Baptist University (FRG2/10-11/101), the Hong Kong Research Grants Council (HKBU202709 and HKUST2/CRF/10), and the Areas of Excellence Scheme from the University Grants Committee of HKSAR, China (project number [AoE/P-03/08]).

[1] a) C. W. Tang, S. A. VanSlyke, *Appl. Phys. Lett.* **1987**, *51*, 913; b) M. A. Baldo, D. F. O'Brien, Y. You, A. Shoustikov, S. Sibley, M. E. Thompson, S. R. Forrest, *Nature* **1998**, *395*, 151; c) M. A. Baldo, M. E. Thompson, S. R. Forrest, *Nature* **2000**, *403*, 750; d) H. Yersin, *Top. Curr. Chem.* **2004**, *241*, 1; e) W. E. Howard, *Sci. Am.* **2004**, *290*, 76; f) P.-T. Chou, Y. Chi, *Chem. Eur. J.* **2007**, *13*, 380; g) P. L. Burn, S.-C. Lo, I. D. W. Samuel, *Adv. Mater.* **2007**, *19*, 1675; h) B. M. W. Langeveld, U. S. Schubert, *Adv. Mater.* **2005**, *17*, 1109; i) W.-Y. Wong, C.-L. Ho, *J. Mater. Chem.* **2009**, *19*, 4457; j) W.-Y. Wong, C.-L. Ho, *Coord. Chem. Rev.* **2009**, *253*, 1709.

[2] a) J. Kido, M. Kimura, K. Nagai, *Science* **1995**, *267*, 1332; b) S. R. Forrest, *Nature* **2004**, *428*, 911; c) H. Wu, L. Ying, W.

Yang, Y. Cao, *Chem. Soc. Rev.* **2009**, *38*, 3391; d) Y. Chi, P. T. Chou, *Chem. Soc. Rev.* **2010**, *39*, 638; e) S. Reineke, F. Lindner, G. Schwartz, N. Seidler, K. Walzer, B. Lüssem, K. Leo, *Nature* **2009**, *459*, 234; f) Q. Wang, D. Ma, *Chem. Soc. Rev.* **2010**, *39*, 2387; g) B. W. D'Andrade, S. R. Forrest, *Adv. Mater.* **2004**, *16*, 1585; h) G. J. Zhou, W.-Y. Wong, S. Suo, *J. Photochem. Photobiol. C: Photochem. Rev.* **2010**, *11*, 133; i) C. H. Chien, C. K. Chen, F. M. Hsu, C. F. Shu, P. T. Chou, C. H. Lai, *Adv. Funct. Mater.* **2009**, *19*, 560; j) Y. You, S. Y. Park, *Dalton Trans.* **2009**, 1267.

[3] a) C.-H. Lin, Y.-Y. Chang, J.-Y. Hung, C.-Y. Lin, Y. Chi, M.-W. Chung, C.-L. Lin, P.-T. Chou, G.-H. Lee, C.-H. Chang, W.-C. Lin, *Angew. Chem.* **2011**, *123*, 3240; *Angew. Chem. Int. Ed.* **2011**, *50*, 3182; b) C.-F. Chang, Y.-M. Cheng, Y. Chi, Y.-C. Chiu, C.-C. Lin, G.-H. Lee, P.-T. Chou, C.-C. Chen, C.-H. Chang, C.-C. Wu, *Angew. Chem.* **2008**, *120*, 4618; *Angew. Chem. Int. Ed.* **2008**, *47*, 4542; c) C.-H. Yang, Y.-M. Cheng, Y. Chi, C.-J. Hsu, F.-C. Fang, K.-T. Wong, P.-T. Chou, C.-H. Chang, M.-H. Tsai, C.-C. Wu, *Angew. Chem.* **2007**, *119*, 2470; *Angew. Chem. Int. Ed.* **2007**, *46*, 2418; d) Y.-H. Song, S.-J. Yeh, C.-T. Chen, Y. Chi, C.-S. Liu, J.-K. Yu, Y.-H. Hu, P.-T. Chou, S.-M. Peng, G.-H. Lee, *Adv. Funct. Mater.* **2004**, *14*, 1221; e) S. Bettington, M. Tavasli, M. R. Bryce, A. Beeby, H. Al-Attar, A. P. Monkman, *Chem. Eur. J.* **2007**, *13*, 1423; f) J. Ding, B. Wang, Z. Yue, B. Yao, Z. Xie, Y. Cheng, L. Wang, X. Jing, F. Wang, *Angew. Chem.* **2009**, *121*, 6792; *Angew. Chem. Int. Ed.* **2009**, *48*, 6664; g) T. Qin, J. Ding, L. Wang, M. Baumgarten, G. Zhou, K. Müllen, *J. Am. Chem. Soc.* **2009**, *131*, 14329; h) S.-C. Lo, R. E. Harding, C. P. Shipley, S. G. Stevenson, P. L. Burn, I. D. W. Samuel, *J. Am. Chem. Soc.* **2009**, *131*, 16681; i) W. Zhu, M. Zhu, Y. Ke, L. Sun, M. Yuan, Y. Cao, *Thin Solid Films* **2004**, *446*, 128; j) C.-H. Yang, C.-H. Chen, I.-W. Sun, *Polyhedron* **2006**, *25*, 2407.

[4] a) M. Cocchi, D. Virgili, V. Fattori, D. L. Rochester, J. A. G. Williams, *Adv. Funct. Mater.* **2007**, *17*, 285; b) J. Kavitha, S.-Y. Chang, Y. Chi, J.-K. Yu, Y.-H. Hu, P.-T. Chou, S.-M. Peng, G.-H. Lee, Y.-T. Tao, C.-H. Chien, A. J. Carty, *Adv. Funct. Mater.* **2005**, *15*, 223; c) C.-M. Che, S.-C. Chan, H.-F. Xiang, M. C. W. Chan, Y. Liu, Y. Wang, *Chem. Commun.* **2004**, 1484; d) S.-C. Lo, G. J. Richards, J. P. J. Markham, E. B. Namdas, S. Sharma, P. L. Burn, I. D. W. Samuel, *Adv. Funct. Mater.* **2005**, *15*, 1451; e) R. N. Bera, N. Cumpstey, P. L. Burn, I. D. W. Samuel, *Adv. Funct. Mater.* **2007**, *17*, 1149; f) G.-J. Zhou, W.-Y. Wong, B. Yao, Z.-Y. Xie, L.-X. Wang, *Angew. Chem.* **2007**, *119*, 1167; *Angew. Chem. Int. Ed.* **2007**, *46*, 1149; g) W.-Y. Wong, C.-L. Ho, Z.-Q. Gao, B.-X. Mi, C.-H. Chen, K.-W. Cheah, Z. Lin, *Angew. Chem.* **2006**, *118*, 7964; *Angew. Chem. Int. Ed.* **2006**, *45*, 7800; h) C. Yang, X. Zhang, H. You, L. Zhu, L. Chen, L. Zhu, Y. Tao, D. Ma, Z. Shuai, J. Qin, *Adv. Funct. Mater.* **2007**, *17*, 651.

[5] a) G. J. Zhou, W.-Y. Wong, X. L. Yang, *Chem. Asian J.* **2011**, *6*, 1706; b) M. C. Gather, A. Köhnen, K. Meerholz, *Adv. Mater.* **2011**, *23*, 233.

[6] a) W.-Y. Wong, G.-J. Zhou, X.-M. Yu, H.-S. Kwok, B.-Z. Tang, *Adv. Funct. Mater.* **2006**, *16*, 838; b) G.-J. Zhou, Q. Wang, C.-L. Ho, W.-Y. Wong, D. Ma, L. Wang, Z. Lin, *Chem. Asian J.* **2008**, *3*, 1830; c) K. Ono, M. Joho, K. Saito, M. Tomura, Y. Matsushita, S. Naka, H. Okada, H. Onnagawa, *Eur. J. Inorg. Chem.* **2006**, 3676; d) J. Nishida, H. Echizen, T. Iwata, Y. Yamashita, *Chem. Lett.* **2005**, *34*, 1378; e) J. Ding, J. Gao, Y. Cheng, Z. Xie, L. Wang, D. Ma, X. Jing, F. Wang, *Adv. Funct. Mater.* **2006**, *16*, 575; f) W.-Y. Wong, Z. He, S.-K. So, K.-L. Tong, Z. Lin, *Organometallics* **2005**, *24*, 4079; g) G.-J. Zhou, X.-Z. Wang, W.-Y. Wong, X.-M. Yu, H.-S. Kwok, Z.-Y. Lin, *J. Organomet. Chem.* **2007**, *692*, 3461; h) C.-L. Ho, W.-Y. Wong, G.-J. Zhou, B. Yao, Z. Xie, L. Wang, *Adv. Funct. Mater.* **2007**, *17*, 2925; i) C.-L. Ho, W.-Y. Wong, Z.-Q. Gao, C.-H. Chen, K.-W. Cheah, B. Yao, Z. Xie, Q. Wang, D. Ma, L. Wang, X.-M. Yu, H.-S. Kwok, Z. Lin, *Adv. Funct. Mater.* **2008**, *18*, 319; j) G. Zhou, Q. Wang, C.-L. Ho, W.-Y. Wong, D. Ma, L. Wang, *Chem. Commun.* **2009**, 3574; k) G.-J. Zhou, C.-L. Ho, W.-Y. Wong, Q. Wang, D. Ma, L. Wang, Z. Lin, T. B. Marder, A. Beeby, *Adv. Funct. Mater.* **2008**, *18*, 499; l) G. Zhou, Q. Wang, X. Wang, C.-L. Ho, W.-Y. Wong, D. Ma, L. Wang, Z. Lin, *J. Mater. Chem.* **2010**, *20*, 7472.

[7] a) S. Lamansky, P. Djurovich, D. Murphy, F. Abdel-Razzaq, H.-E. Lee, C. Adachi, P. E. Burrows, S. R. Forrest, M. E. Thompson, *J. Am. Chem. Soc.* **2001**, *123*, 4304; b) A. Tsuboyama, H. Iwawaki, M. Furugori, T. Mukaide, J. Kamatani, S. Igawa, T. Moriyama, S. Miura, T. Takiguchi, S. Okada, M. Hoshino, K. Ueno, *J. Am. Chem. Soc.* **2003**, *125*, 12971; c) K. Dedeian, J. Shi, N. Shepherd, E. Forsythe, D. C. Morton, *Inorg. Chem.* **2005**, *44*, 4445; d) S.-C. Lo, C. P. Shipley, R. N. Bera, R. E. Harding, A. R. Cowley, P. L. Burn, I. D. W. Samuel, *Chem. Mater.* **2006**, *18*, 5119; e) S. Jung, Y. Kang, H.-S. Kim, Y.-H. Kim, C.-L. Lee, J.-J. Kim, S.-K. Lee, S.-K. Kwon, *Eur. J. Inorg. Chem.* **2004**, 3415; f) C.-L. Li, Y.-J. Su, Y.-T. Tao, P.-T. Chou, C.-H. Chien, C.-C. Cheng, R.-S. Liu, *Adv. Funct. Mater.* **2005**, *15*, 387; g) X. Li, B. Minaev, H. Ågren, H. Tian, *J. Phys. Chem. C* **2011**, *115*, 20724; h) X. Li, B. Minaev, H. Ågren, H. Tian, *Eur. J. Inorg. Chem.* **2011**, 2517.

[8] a) T. A. Clem, D. F. J. Kavulak, E. J. Westling, J. M. J. Frechet, *Chem. Mater.* **2010**, *22*, 1977; b) W.-Y. Wong, S.-M. Chan, K.-H. Choi, K.-W. Cheah, W.-K. Chan, *Macromol. Rapid Commun.* **2000**, *21*, 453; c) M. Zhang, H. Fan, X. Guo, Y. He, Z.-G. Zhang, J. Min, J. Zhang, G. Zhao, X. Zhan, Y. Li, *Macromolecules* **2010**, *43*, 8714; d) T. Yamamoto, H. Suganuma, T. Maruyama, T. Inoue, Y. Muramatsu, M. Arai, D. Komarudin, N. Ooba, S. Tomaru, S. Sasaki, K. Kubota, *Chem. Mater.* **1997**, *9*, 1217; e) W.-Y. Wong, K.-H. Choi, G.-L. Lu, Z. Lin, *Organometallics* **2002**, *21*, 4475; f) W.-Y. Wong, X.-Z. Wang, Z. He, K.-K. Chan, A. B. Djurišiá, K.-Y. Cheung, C.-T. Yip, A. M.-C. Ng, Y. Y. Xi, C. S.-K. Mak, W.-K. Chan, *J. Am. Chem. Soc.* **2007**, *129*, 14372.

[9] a) S. Lamansky, P. Djurovich, D. Murphy, F. Abdel-Razzaq, R. Kwong, I. Tsyba, M. Bortz, B. Mui, R. Bau, M. E. Thompson, *Inorg. Chem.* **2001**, *40*, 1704; b) S. Okada, K. Okinaka, H. Iwawaki, M. Furugori, M. Hashimoto, T. Mukaide, J. Kamatani, S. Igawa, A. Tsuboyama, T. Takiguchi, K. Ueno, *Dalton Trans.* **2005**, 1583.

[10] a) A. C. Stückl, U. Klement, K.-J. Range, *Z. Kristallogr.* **1993**, *208*, 297; b) T. J. Giordano, P. G. Rasmussen, *Inorg. Chem.* **1975**, *14*, 1628.

[11] a) M. Ghedini, D. Pucci, A. Crispini, G. Barberio, *Organometallics* **1999**, *18*, 2116; b) H. Katoh, K. Miki, Y. Kai, N. Tanaka, N. Kasai, *Bull. Chem. Soc. Jpn.* **1981**, *54*, 611; c) J. Brooks, Y. Babayan, S. Lamansky, P. I. Djurovich, I. Tsyba, R. Bau, M. E. Thompson, *Inorg. Chem.* **2002**, *41*, 3055.

[12] P.-I. Kvam, M. V. Puzyk, K. P. Balashev, J. Songstad, *Acta Chem. Scand.* **1995**, *49*, 335.

[13] G.-J. Zhou, Q. Wang, W.-Y. Wong, D. Ma, L. Wang, Z. Lin, *J. Mater. Chem.* **2009**, *19*, 1872.

[14] K. A. King, P. J. Spellane, R.-J. Watts, *J. Am. Chem. Soc.* **1985**, *107*, 1431.

[15] a) M. Thelakkat, H.-W. Schmidt, *Adv. Mater.* **1998**, *10*, 219; b) R. S. Ashraf, M. Shahid, E. Klemm, M. Al-Ibrahim, S. Sensfuss, *Macromol. Rapid Commun.* **2006**, *27*, 1454.

[16] *SAINT+*, v. 6.02a, Bruker Analytical X-ray System, Inc., Madison, WI, **1998**.

[17] G. M. Sheldrick, *SADABS*, Empirical Absorption Correction Program, University of Göttingen, Germany, **1997**.

[18] G. M. Sheldrick, *SHELXTL*™, reference manual, v. 5.1, Madison, WI, **1997**.

[19] a) W. R. Wadt, P. J. Hay, *J. Chem. Phys.* **1985**, *82*, 284; b) P. J. Hay, W. R. Wadt, *J. Chem. Phys.* **1985**, *82*, 299.

[20] M. J. Frisch, G. W. Trucks, H. B. Schlegel, G. E. Scuseria, M. A. Robb, J. R. Cheeseman, J. A. Montgomery, T. Vreven Jr, K. N. Kudin, J. C. Burant, J. M. Millam, S. S. Iyengar, J. Tomasi, V. Barone, B. Mennucci, M. Cossi, G. Scalmani, N. Rega, G. A. Petersson, H. Nakatsuji, M. Hada, M. Ehara, K. Toyota,

R. Fukuda, J. Hasegawa, M. Ishida, T. Nakajima, Y. Honda, O. Kitao, H. Nakai, M. Klene, X. Li, J. E. Knox, H. P. Hratchian, J. B. Cross, C. Adamo, J. Jaramillo, R. Gomperts, R. E. Stratmann, O. Yazyev, A. J. Austin, R. Cammi, C. Pomelli, J. W. Ochterski, P. Y. Ayala, K. Morokuma, G. A. Voth, P. Salvador, J. J. Dannenberg, V. G. Zakrzewski, S. Dapprich, A. D. Daniels, M. C. Strain, O. Farkas, D. K. Malick, A. D. Rabuck, K. Raghavachari, J. B. Foresman, J. V. Ortiz, Q. Cui, A. G. Baboul, S. Clifford, J. Cioslowski, B. B. Stefanov, G. Liu, A. Liashenko, P. Piskorz, I. Komaromi, R. L. Martin, D. J. Fox, T. Keith, M. A. Al-Laham, C. Y. Peng, A. Nanayakkara, M. Challacombe, P. M. W. Gill, B. Johnson, W. Chen, M. W. Wong, C. Gonzalez, J. A. Pople, *Gaussian 03*, rev. B05, Gaussian, Inc., Pittsburgh, PA, **2003**.

[21] R. Pis Diez, *MullPop*, The National University of La Plata, Argentina.

[22] G. Schaftenaar, *Molden* v3.7, CAOS/CAMM Center Nijmegen, Toernooiveld, Nijmegen, The Netherlands, **2001**.

Received: January 22, 2012
Published Online: March 16, 2012

